

## Advanced glycation end-products: mechanics of aged collagen from molecule to tissue

Alfonso Gautieri<sup>a,b,c,1</sup>, Fabian S. Passini<sup>a,b,1</sup>, Manuel Guizar-Sicairos<sup>d</sup>, Giulia Carimati<sup>e</sup>, Piero Volpi<sup>e</sup>, Matteo Moretti<sup>f</sup>, Alberto Redaelli<sup>c</sup>, Martin Berli<sup>a</sup>, Jess G. Snedeker<sup>a,b,2</sup>

<sup>a</sup> Department of Orthopedics, Balgrist University Hospital, University of Zurich, 8008 Zurich, Switzerland

<sup>b</sup> Institute for Biomechanics, ETH Zurich, 8093 Zurich, Switzerland

<sup>c</sup> Department of Electronics, Information and Bioengineering, Politecnico di Milano, Piazza Leonardo da Vinci 32, 20133 Milano, Italy

<sup>d</sup> Paul Scherrer Institute, 5232 Villigen PSIVilligen, Switzerland

<sup>e</sup> Department of Knee Orthopedic and Sports Traumatology Unit, Humanitas Research Hospital, 20089 Rozzano, Italy

<sup>f</sup> IRCCS Ist Ortoped Galeazzi, Cell & Tissue Engineering Lab, 20161 Milan, Italy

<sup>1</sup> These authors contributed equally

<sup>2</sup> To whom correspondence should be addressed:

Prof. Jess G. Snedeker

Uniklinik Balgrist / ETH Zurich

Lengghalde 5 8008 Zurich

Tel: +41 44 510 73 30

Email: jsnedeker@research.balgrist.ch

## **ABSTRACT**

Concurrent with a progressive loss of regenerative capacity, connective tissue aging is characterized by a progressive accumulation of Advanced Glycation End-products (AGEs). Besides being part of the typical aging process, type II diabetics are particularly affected by AGE accumulation due to abnormally high levels of systemic glucose that increases the glycation rate of long-lived proteins such as collagen. Although AGEs are associated with a wide range of clinical disorders, the mechanisms by which AGEs contribute to connective tissue disease in aging and diabetes are still poorly understood. The present study harnesses advanced multiscale imaging techniques to characterize a widely employed *in vitro* model of ribose induced collagen aging and further benchmarks these data against experiments on native human tissues from donors of different age. These efforts yield unprecedented insight into the mechanical changes in collagen tissues across hierarchical scales from molecular, to fiber, to tissue-levels. We observed a linear increase in molecular spacing (from 1.45 nm to 1.5 nm) and a decrease in the D-period length (from 67.5 nm to 67.1 nm) in aged tissues, both using the ribose model of *in vitro* glycation and in native human probes. Multiscale mechanical analysis of *in vitro* glycated tendons strongly suggests that AGEs reduce tissue viscoelasticity by severely limiting fiber-fiber and fibril-fibril sliding. This study lays an important foundation for interpreting the functional and biological effects of AGEs in collagen connective tissues, by exploiting experimental models of AGEs crosslinking and benchmarking them for the first time against endogenous AGEs in native tissue.

**Keywords:** Collagen Mechanics, Advanced glycation end-products, Functional Microscopy, small-angle X-ray scattering, Aging

## 1. INTRODUCTION

Among the many age- and diabetes-related functional changes affecting human tissues there is a characteristic increase in rates of tissue injury with concurrently reduced healing capacity [1]. While the causes of these changes are multifactor, the accumulation of non-enzymatic crosslinks within the family of advanced glycation end-products (AGEs) is increasingly thought to play a role [2]. Formation of AGEs is both spontaneous and quite slow, affecting only proteins with relatively long half-lives and which contain exposed lysine residues [3-6]. In these respects, fibrillar collagens are highly susceptible to glycation. While collagen half-life varies between tissues it remains considerably long, ranging from 1 to 2 years for type I collagen in bone, to 10-15 years in skin, and over 100 years for the type II collagens in cartilage [7-9]. Aside from protein longevity, another factor that influences the formation of AGEs is the base level of glucose in the bloodstream. Hyperglycemia related to diabetes is thus a second important cause of AGE formation and accumulation [10, 11].

Biochemically, the glycation reaction initiates with the formation of a reversible Schiff base between a carbohydrate, typically glucose or ribose [12], and a protein amino group (e.g., a lysine side-chain). The unstable Schiff base becomes a stable keto amine intermediate, usually referred to as Amadori product. Over the course of months or years a complex series of reactions eventually can lead to formation of various AGEs, which can be either protein adducts or crosslinks (Fig. 1A) [13]. Recently, it has been found that among all different AGEs in human tissues the most abundant is glucosepane, a lysine-arginine cross-linking product [14, 15].

Functionally, AGEs have been implicated in a range of deleterious physiological effects that can be divided into two major categories. On one hand, they alter molecular recognition [16] by modifying the biochemistry of specific protein binding sites [17]. On the other hand, AGEs crosslinks such as glucosepane are known to alter the mechanical properties of load bearing proteins such as collagen [18, 19], leading to stiffer tissues and decreased viscoelasticity [20-22]. Both these alterations at the molecular level can participate in generating a cascade of adverse effects including arterial stiffening [23], atherosclerosis [24], nephropathy [25], retinopathy [26] and neuropathy [27]. From the biomechanical standpoint, intermolecular cross-links are known to increase tissue stiffness, mechanical load to failure and denaturation temperatures of collagen tissue. At the same time reduced mechanical robustness of AGE crosslinked tissue has been observed in animals [28, 29] and in humans [30, 31]. Because collagen tissue biology is so intimately related to extracellular matrix mechanics, AGE crosslinks may potentially drive the progression of connective tissue disease [2].

Although macroscopic AGEs-mediated changes in collagen tissue properties have long been recognized, the functional and molecular consequences are yet to be fully elucidated. It has been suggested that glycation primarily affects collagen fibrils at their surface (Fig. 1B), due to the dense packing of collagen fibrils [32]. However, the molecular sites and hierarchical level at which AGEs are likely to accumulate within a tissue remains poorly understood. Previous studies from our group showed drastically decreased tendon viscoelasticity and brittle failure mode in tendons treated with methylglyoxal (MGO, a strong cross-linking agent) [33]. In bone the accumulation of AGEs has been correlated to decreased bone toughness and increased fracture risk [34, 35]. Although the role of AGEs has been investigated mostly at the tissue level, a few studies reported AGE-related mechanical changes in collagen fibrils of tendon tissue. Our group [36] found a higher failure resistance in MGO treated collagen fibrils as well as a reduction in the lateral sliding of collagen molecules within fibrils, while fibril modulus remained unchanged. Svensson et al. [21] observed

a three-phase behavior pattern in the stress-strain curves of human collagen fibrils. An initial increase in modulus was followed by a plateau phase and then by a final rise in modulus. The third region (stiffening before failure) was not noticed in the collagen fibrils from rat tail tendons. Since a higher AGEs content was detected in human fibrils, such mechanical changes have been suggested to be a consequence of glycation.

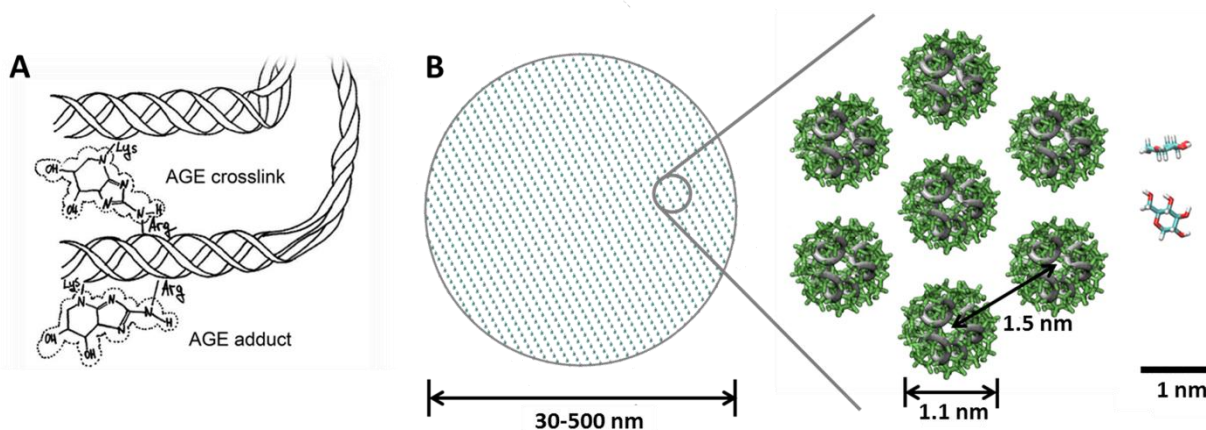


**Figure 1. Collagen and AGEs structures.** Adducts and crosslinking AGEs on collagen molecule (A). Structure and size of collagen fibril and glycating sugars (B). Collagen fibrils (size is in the range 30-500 nm) are assemblies of collagen molecules with diameter of  $\approx 1.1$  nm and that are separated by a molecular distance of  $\approx 1.5$  nm [37, 38]. This dense packing leaves little room for reducing sugar such as glucose or ribose (on the right, to scale) to penetrate within the fibril, suggesting that most of the glycation is likely to occur on the surface of the fibril or between different fibrils.

In the current work we investigate the effects of physiologically relevant AGEs on collagen tissue mechanics, by combining multi-scale imaging and mechanical testing techniques. These experiments focus at the fiber and molecular scales, using advanced light microscopy and small-angle X-ray scattering (SAXS) techniques, respectively. In a first step, these methods were harnessed to comprehensively characterize *in vitro* tissue glycation by ribose as reducing agent, with these findings then being benchmarked against the more limited experiments that were possible on tissues obtained from human donors across a wide range of age. We report here unprecedented quantitative insight that was gained from these experiments, better illuminating the molecular mechanisms and mechanical effects of AGE collagen crosslinking in the dense collagen connective tissue of tendon.

## 2. RESULTS

### 2.1 Tissue glycation increased fluorescence associated to AGE formation in a dose dependent manner.

Fluorometric assay was carried out after enzymatic papain digestion, in order to verify the glycation levels of the collagen tissues. Significant differences were detected between non-glycated and glycated rat tail tendon samples at all time points (3, 6 and 11 days,  $p < 0.05$ ). Tendons treated with ribose showed a gradual increase in pentosidine-related fluorescence (328/378 nm) and exhibited over three-time higher fluorescence signal at 11 days incubation compared to controls (Fig. 2).

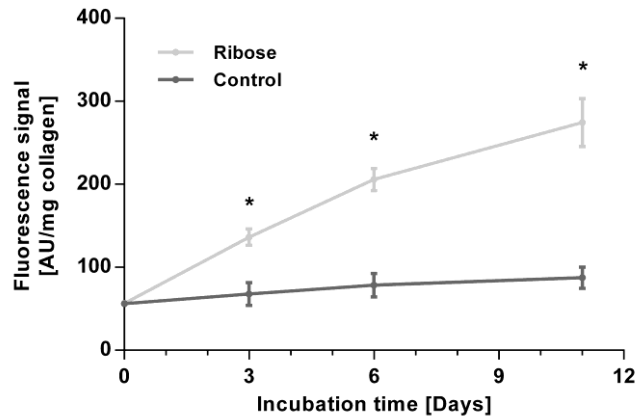


**Figure 2. Evidences of AGEs formation.** Fluorescence was measured with wavelengths associated with pentosidine (ex 328, em 378). Specimens were normalized by the dry weight of the samples ( $n = 5$ ).

## 2.2 Tissue level failure behavior and stress relaxation but not elasticity were affected by tissue glycation.

We observed that ribose treatment heavily affected the mechanical behavior of collagen tissue during ramp to failure experiments (Fig. 3A). A key feature is the total loss of post yield plastic behavior, typically characterized by a long plateau in the stress-strain curve after inflection at the yield point. The elastic modulus was not significantly affected in the glycated group. Conversely, the ultimate stress was considerably higher (+83%,  $p < 0.01$ ) and the failure strain was reduced (-22%,  $p < 0.01$ ).

Viscoelastic properties were studied by applying an incremental stretching protocol (0-6%  $L_0$  at 0.6%  $L_0$  increments, 200s of relaxation period) to paired fascicles ( $n = 8$ ) after incubating them either in ribose supplemented medium or in control medium for 12 days. We observed a significant decrease of stress relaxation at all applied strain intervals ( $p < 0.01$ ) after ribose treatment (Fig. 3B).

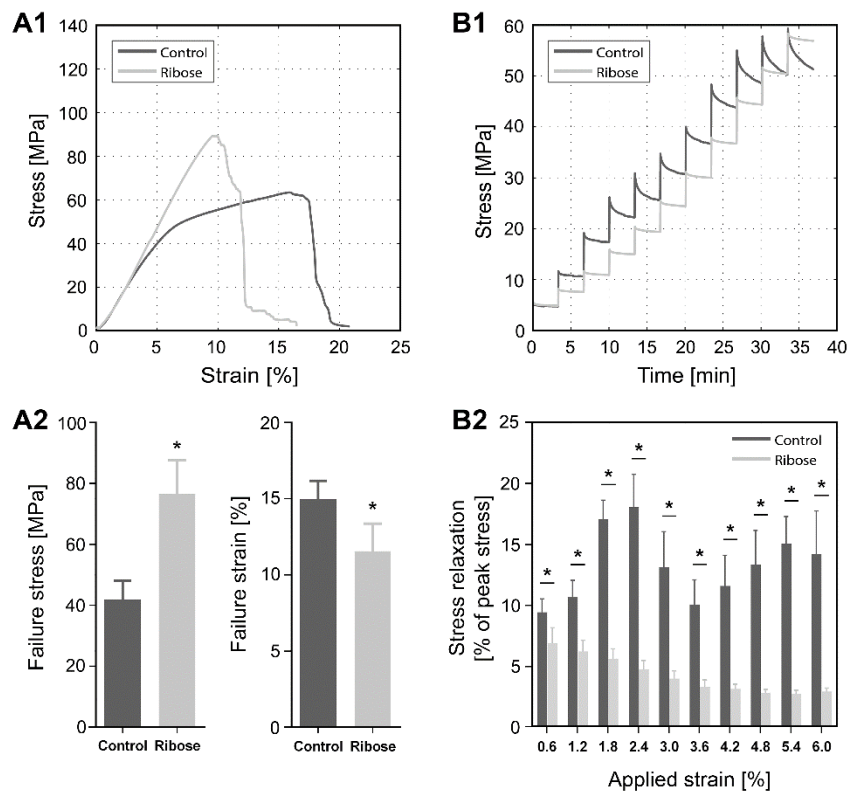


**Figure 3. Glycation-induced effects on tissue mechanical properties.** (A1) Representative stress–strain plot from fascicle mechanics testing ( $n = 8$ ). (A2) Changes in mechanical properties by cross-linking. (B1) Representative stress–time relations of a control sample and a ribose-treated sample ( $n = 8$ ). (B2) Averaged ( $\pm$  SD) stress decay at each applied incremental strain. \* indicates statistically significant differences.

### 2.3 Fiber level sliding mechanics are dramatically diminished by tissue glycation.

Fiber mechanics was investigated using photobleached lines that were taken with a confocal microscope prior the relaxation experiments. Z-stacks of the collagen matrix with photobleached lines were acquired to study fiber kinematics between strain intervals. Analysis of fiber deformations within individual fascicles revealed significantly increased fiber strain in the latter half of the stretching protocol and drastically reduced fiber-fiber sliding by the ribose treatment (see Fig. 4 and movie in Supplementary Information).

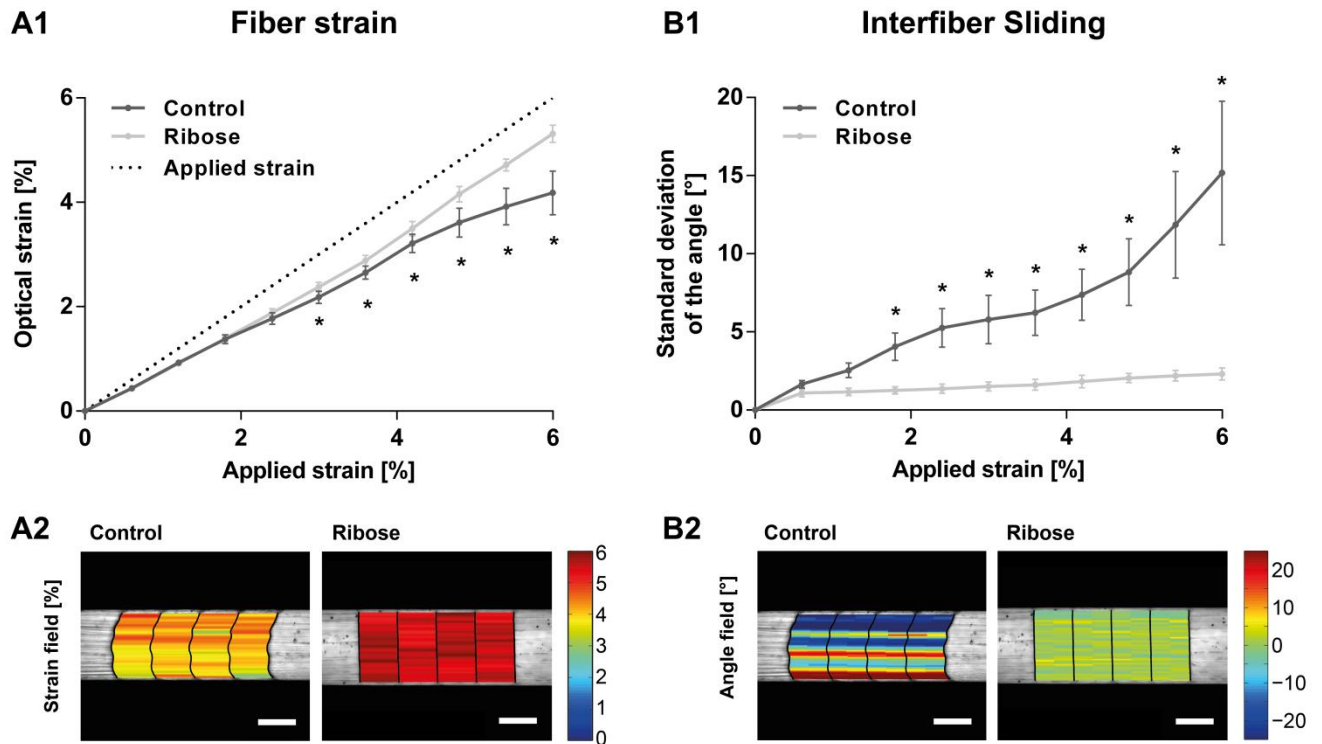


**Figure 4. Fiber kinematics affected by ribose-induced glycation.** Fiber strain (A) and interfiber sliding (B) between strain increments were determined from the displacements of the photobleached lines on the extracellular matrix ( $n = 8$ ). Representative strain (A2) and angle fields (B2) measured at 6%  $L_0$  applied strain. Photobleached lines of the non-glycated fascicle display a typical waviness, in sharp contrast the photobleached lines of the ribose-treated (glycated) fascicle remain nearly straight throughout the entire stretching experiment. \* indicates statistically significant differences ( $p < 0.05$ ) and scale bars represent 100  $\mu\text{m}$ .

#### 2.4 Reduced viscoelastic behavior was also confirmed at the fibril level scale.

Collagen fibril deformation was measured as absolute and relative increase of D-periodic length. Data indicated that the glycation induced changes in mechanical behavior at the tissue level was reflected in a change in deformation mechanism at the fibril level (Fig. 5A,B). In the control samples the fibril deformed linearly up to  $D \approx 70$  nm, when the yield point was reached. After this point the equatorial peaks disappeared (i.e., the D-banding is disrupted) and the tissue entered in the plastic regime before failure. Conversely, glycated samples show a decreased D-period at rest (Fig. 5C) and deformed up to  $D \approx 72$  nm (Fig. 5D,E), where tissue failed with a characteristically brittle behavior. The glycated fibrils sustained a larger share of tissue deformation (80%), while fibrils in the control samples sustained  $\approx 60\%$  of total tissue strain and the ratio was further reduced at larger strain (Fig. 5F).

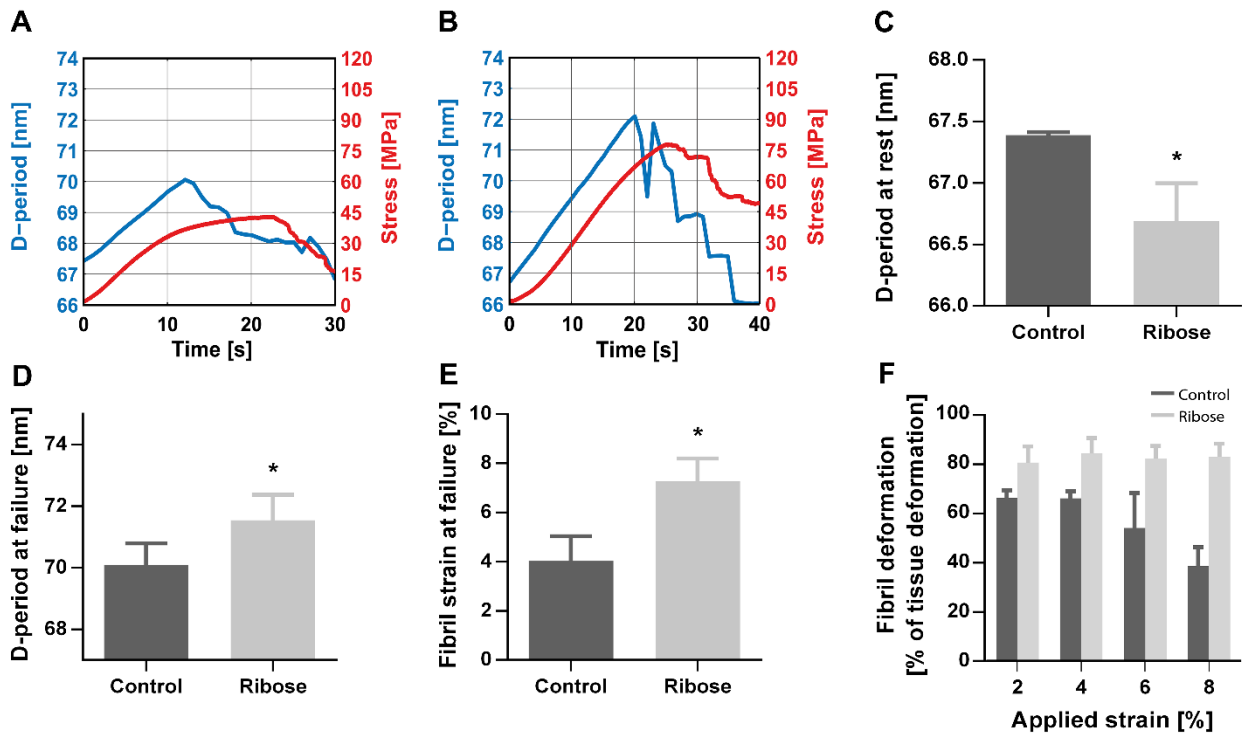


**Figure 5. Fibril level ramp-to-failure.** Plots of the length of D-period and tissue stress as a function of time for control samples (A) and glycosylated samples (B) during ramp to failure experiments. The plots show that the changes in stress-time curves are due to changes in deformation mechanisms at the fibril level. In particular, glycosylated samples show a decreased D-period at rest (C), a larger D-period at failure (D) and consequently a larger fibrillary deformation (E). The glycosylated fibrils sustain a larger share of tissue deformation (80%), while fibrils in the control samples sustain  $\approx 60\%$  of total tissue strain and the ratio is further reduced at larger strain (F).

The reduced viscoelastic behavior observed at the tissue and fiber scale was also confirmed at the fibril level scale. The length of the D-period was monitored during stress-relaxation tests (180 s relaxation time, from  $0.6\%L_0$  to  $3.0\%L_0$ ) (Fig. 6A). The stress relaxation observed for control samples was strictly related to the high degree of fibril-fibril sliding, which leads to a partial recovery of the D-period initial length. Conversely, the non-enzymatic crosslinks introduced by ribose incubation lead to a total loss of fibril sliding and hence the lack of D-period relaxation (Fig. 6B).

We further investigated the ability of collagen samples to recover the fibrillar organization (i.e., D-period) after stretching to  $4\%L_0$ ,  $8\%L_0$  and  $12\%L_0$ . We observed that the control samples were able to recover the initial length of the D-period after the removal of the load, even if during the stretching to larger deformation the D-banding temporarily disappeared (see Fig. S1A in Supplementary Information). However, the intensity of the 3<sup>rd</sup> equatorial peak showed a marked decrease following the stretching to  $8\%L_0$  and  $12\%L_0$ , suggesting damage to the tissue integrity. Conversely, glycosylated samples were able to recover the length of the D-period after load removal but also the intensity of the 3<sup>rd</sup> peak was unaffected (Fig. S1B), suggesting that the samples were largely undamaged by deformations up to  $12\%L_0$ .

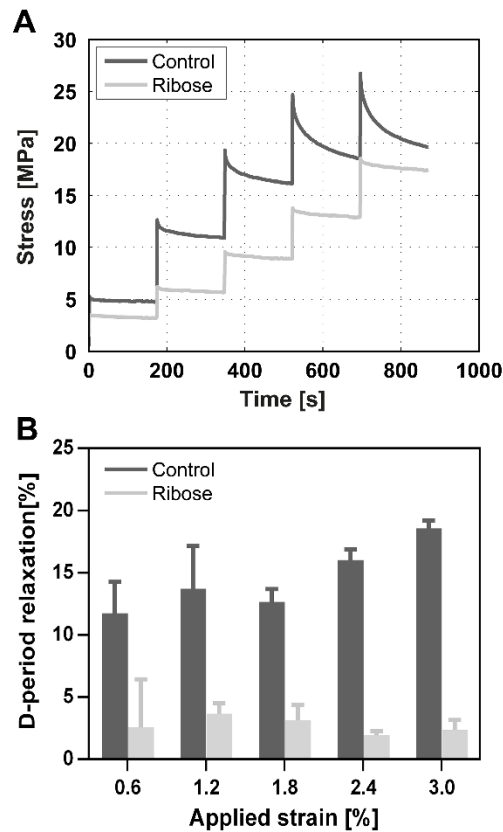


**Figure 6. Fibril level stress relaxation.** Plot of D-period length as a function of time during stress relaxation experiments (A). Glycated samples showed a greatly reduced D-period relaxation (< 5%) compared to control samples (B).

### 2.5 Completely different loading mechanisms at the sub-fibrillar level after glycation.

The ratio of intensities of the 2<sup>nd</sup> and 3<sup>rd</sup> order reflections was analyzed to assess changes in length of the overlap region and gap region during the ramp-to-failure experiments [36, 39]. The control fibrils showed three distinct loading mechanism at the sub-fibrillar scale (Fig. 7A,B). In the first phase the fibril deformation took place only in the gap region, while the overlap region was unaffected. Onset of the second phase was observed when the D-period reached a value of 68.5 nm (which occurred halfway in the linear region of the stress-time curve). In this phase the gap was observed to increase while the overlap decreased. Finally, when the D-period reached a mean value of 70.2 nm the D-banding was apparently lost and the tissue entered into a plastic regime before failure.

Throughout the whole ramp-to-failure experiment, glycated samples exhibited a single deformation mechanism by which the D-period increased, likely due to a concurrent increase of the gap region and to a smaller extent a decrease of the overlap region (Fig. 7C,D). When the D-period reached a mean value of 72.2 nm, the equatorial reflections disappeared, indicating a loss of D-banding that was rapidly followed by tissue failure, without the plastic plateau observed in the control group.

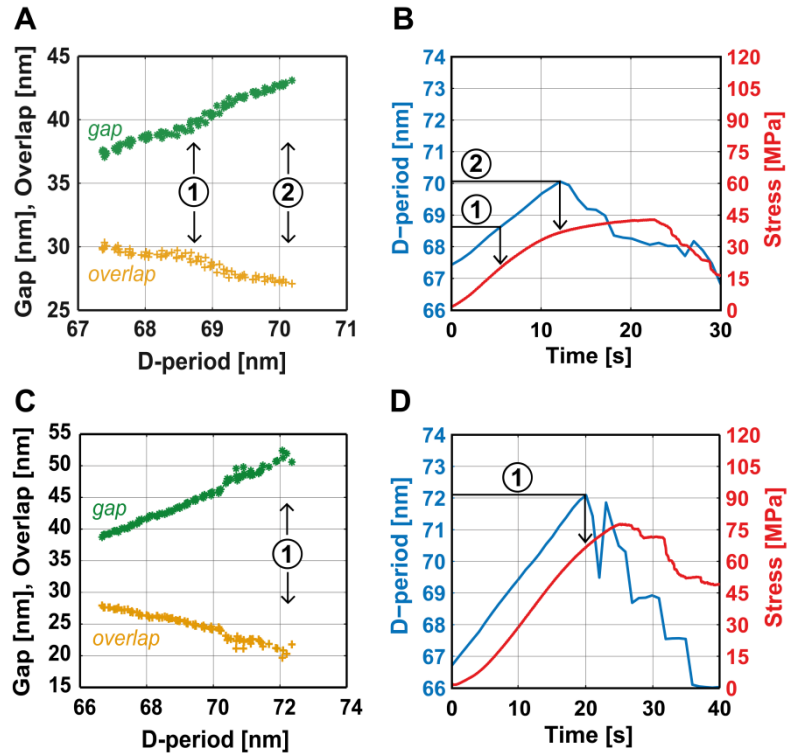


**Figure 7. Fibrillar deformation mechanisms.** The ratio of the integrated intensities for the 2<sup>nd</sup> and 3<sup>rd</sup> order equatorial collagen reflections were used to determine the relative contribution of gap and overlap regions to the D-period deformation for control samples (A, B) and glycated samples (C,D). During the ramp to failure experiment, the control fibrils showed a first phase in which only the gap region (red) carried the deformation, while the overlap region (blue) was largely unchanged. This phase ended (1) when the D-period reached a value of 68.5 nm, which corresponded to the first half of the linear region in the stress-time curve (B). In a second phase the gap increased while the overlap decreased. This phase ended when the D-period reached 70.2 nm (2), which corresponded to the yield point. After this point the equatorial SAXS diffractions disappeared with the stress-strain curves entered into a plastic regime before failure. In contrast, the overlap region glycated fibrils (panel C in blue) decreased from the start of the loading test, and the tissue showed a single subfibrillar loading mechanism before the D-period was lost (point (1), at 72.2 nm), which corresponds to the failure of the tissue (D).

## 2.6 Human tissue display characteristic D-banding and molecular spacing observed *in vitro*.

In order to further investigate the effect of glycation and AGE crosslinks on collagen mechanics we performed SAXS-coupled mechanical tests on human tendon tissues (n=25), with donor ages ranging from 16 to 89 year and thus with different degrees of AGEs accumulation. The level of glycation was semi-quantitatively tested through fluorescence analysis. The results showed a strong correlation between donor age and pentosidine-related fluorescence ( $R^2 = 0.642$ ,  $p < 0.01$ ) (Fig. 8A). The tissue-level mechanical data (i.e., elastic modulus, yield stress, yield strain, failure stress, failure strain) were highly scattered, with no direct correlation to donor age (Fig. S2). Concerning the fibril-level characterization from SAXS data, the older human tissues showed a clear decrease in length of the D-period at rest (Fig. 8B), from  $\approx 67.5$  nm at younger ages to  $\approx 67.0$  nm at the oldest aged specimens ( $R^2 = 0.477$ ,  $p < 0.01$ ). This is in line with observed behavior in glycated RTTFs versus controls. The molecular distance at rest showed a clearly increasing trend ( $R^2 = 0.784$ ,  $p < 0.01$ ) with donor age, ranging from  $\approx 1.45$  nm at younger age to  $\approx 1.5$  nm at older age (Fig. 8C). A similar increase in molecular distance is observed for the *in vitro* glycated RTTFs. However, the high variability in the human data and low number of specimens precluded confirmation of the mechanical

effects at the fibril level observed using the highly controlled RTTF *in vitro* glycation model (e.g., larger fibril deformation at failure or lack of fibril relaxation) (Fig. S3).

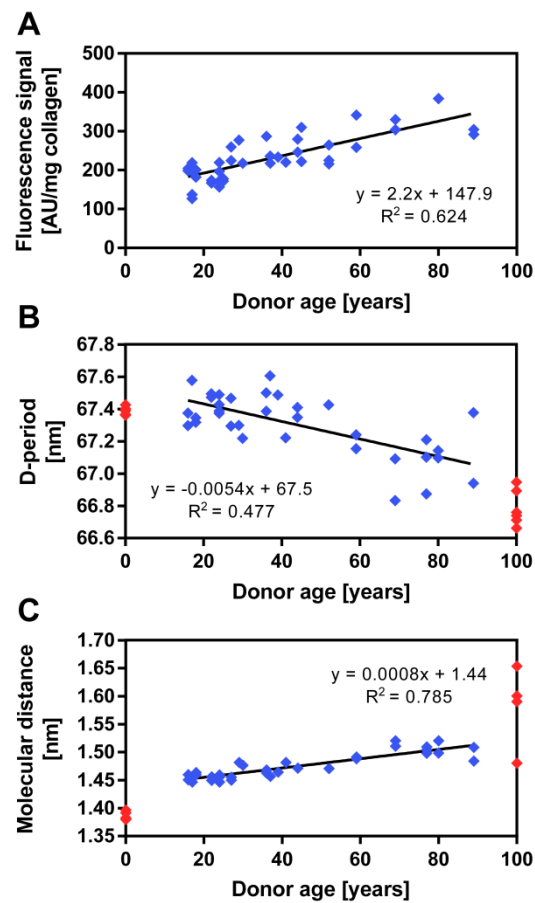


**Figure 8. Glycation effects in vivo.** Fluorescence levels (arbitrary units normalized by the dry weight of the samples) as a function of donor age, assessed with the set of wavelength associated to pentosidine (A). Age and glycation led to a clear decrease of fibrillar D-period (B) and to an increase of molecular spacing (C), consistent with observations from *in vitro* glycation experiments depicted in the plot with red marks at “age 0” (control samples) and “age 100” (glycated samples).

### 3. DISCUSSION

Advanced glycation end-products can dramatically affect collagen tissue viscoelasticity and molecular deformation [36]. On the basis of our early findings, the present study sought to clarify mechanisms behind these behaviors and verify that they occur in naturally aged, native tissue. We comprehensively investigated AGE mechanical effects at different hierarchical levels of tendon, from the tissue to fiber, to fiber-fiber interactions, to fibril-fibril interactions, and ultimately at the sub-fibril scale. In these experiments we used ribose as *in vitro* glycation agent to induce AGEs formation. Ribose has a substantially higher reactivity compared to glucose that facilitates its value as an experimental model and further has the ability to prevalently form pentosidine, a physiologically relevant fluorescent lysine-arginine crosslink [13]. We then compared the results obtained with *in vitro* glycation against those obtained using human tendon specimens from donors spanning a wide range of age. Aged human tissues are known to

progressively accumulate AGEs over time, due to the irreversible nature of non-enzymatic crosslinking and low turnover of collagen.

At the tissue level, ribose cross-linked specimens showed a clear loss of stress relaxation behavior, which is consistent with our previous studies [36, 40] where AGEs were induced by methylglyoxal treatment, a substantially more reactive compound. This reduction in viscoelasticity can be attributed to changes at lower hierarchical levels, i.e. the fiber and the fibril levels.

At the fiber level, we used confocal microscopy techniques to quantify fiber kinematics from the displacements of photobleached lines [41-43] in response to tissue-level mechanical stretch. This scale level is particularly of interest, as cell-matrix interaction and the associated mechanotransduction are likely to be affected by matrix glycation. A key quantitative finding of the present work is the markedly reduced fiber-fiber sliding after ribose glycation, as detected by analyzing the fiber kinematics between strain intervals. Photobleached fiducial marking lines on non-glycated fascicles exhibited a pronounced undulation (a proxy for interfiber sliding), in sharp contrast the photobleached lines on the glycated fascicles displayed a nearly complete lack of sliding as indicated by their remaining practically straight throughout the entire experiment (Fig. 4). In addition, analysis at higher applied strains of the matrix revealed a considerable increase in fiber strain in cross-linked fascicles compared to the control fascicles, consistent with the physical compensation for any loss of fiber-fiber sliding [40].

Small-angle X-ray scattering was used to determine the effect of glycation at the fibril level. The key, and previously unknown, finding of the present work was the observation of significant loss of fibril-fibril sliding that lead to a substantially altered tissue deformation mechanism that is largely based on the elastic deformation of the fibrils until brittle failure of the tissue (Fig. 5F). Indeed, in control samples the fibrillar deformation represented 40-60% of the total deformation of the tissue, whereas in glycated samples the fibril deformation reached levels beyond 80% of the tissue deformation. Similarly, glycated samples did not show D-period recovery during stress relaxation experiments (Fig. 6) suggesting the suppression of viscous sliding between fibrils. The fibril deformation mechanism was also drastically affected (Fig. 7). The control samples showed three distinct deformation mechanisms, characterized by (1) increase of gap region, (2) increase of gap region concurrent to a decrease of overlap region and (3) loss of D-banding (corresponding to the post-yield plastic regime). Conversely, glycated samples showed a unique (and previously unknown/unreported) deformation mechanism with the concurrent increase of gap region and decrease of overlap region until the loss of D-banding, which corresponds to the sample brittle failure.

Beyond the identification of previously unknown glycation driven changes in collagen deformation mechanisms, we ran what is to our knowledge the first series of SAXS-coupled mechanical tests on human tendon samples aiming to characterize effects that *in vivo* collagen glycation during the aging process may have on collagen function. The aim was to compare these results to those of the *in vitro* glycation model. Interestingly, the human tissue SAXS data confirmed the decrease of D-period length and the increase of molecular spacing observed using the *in vitro* glycation models (Fig. 8), providing a valuable confirmation of their physiological relevance. These effects were highly consistent across samples, a striking fact considering the extremely large macroscopic and microscopic variability between donor tissue that precluded meaningful statistical comparison to other effects induced by *in vitro* glycation.

Inability to draw clear conclusions from the presented data on human tissues under mechanical load is not only attributed to biological variability, but particularly to difficulty in specimen dissection and handling.

Indeed, while intact functional tendon units are easily extracted from a rat tail with a geometry that can be straightforwardly characterized, the isolation of fascicles from human samples is nearly impossible without damaging them. We thus resorted to cutting small strips of tendon tissue, which although geometrically reproducible also leads to partial and unavoidable tissue damage that adds substantial noise to SAXS based measurements. These factors are expected to play at least a minor role in the high experimental variability in the mechanical loading tests, compared to the clear cSAXS findings obtained for the unloaded samples.

Although a few preferential sites for AGE formation have been discovered at the molecular level [17], the location of AGEs within the tissue itself until now remained unclear. Our work strongly supports that glycation primarily affects fibril-fibril and fiber-fiber sliding and thus the surface of the fibrils (although the increase in molecular distance implies diffusion of glucose within the fibril). The alteration of fibril surface properties and behavior could potentially affect the cell-collagen binding and the associated focal adhesion mediated signaling, the behavior of the stretch activated ion channels (SACs) and sliding activation of the primary cilium, as well as the manner in which the nucleus deforms under mechanical stress [44]. Those mechanisms and pathways may play a crucial role in the mechanotransduction of tendon cells, therefore it is feasible that changes in the extracellular matrix can have adverse effects on the cell-mediated tissue homeostasis and repair. The fact that glycation occurs primarily on the fibril surface and thus at an accessible location could have also important implication for therapeutic strategies based on enzymatic deglycation [45, 46].

The present study has some limitations that must be considered. First, the formation of AGEs and cross-links induced by ribose treatment was not directly quantified, however previous investigations have provided direct molecular evidence for pentosidine formation in tissue incubated with ribose [47, 48]. Additionally, in this work the indirect measurements of AGE formation by fluorescence showed clear changes after ribose treatment, comparable to the previous reports [47-49]. A further potential weakness concerns the physiological importance of the *in vitro* established aging-model. The high ribose concentrations used to acutely induce AGE cross-links are non-physiological and the incubation period does not directly represent the *in vivo* glycation process. Therefore, cell-based matrix adaptations that would take place *in vivo* as a reaction to the AGE accumulation were not considered in this study. However, the employed aging-model prevents critically confounding factors, e.g. due to loss of collagen, diseases and lifestyle. Hence, future study should be directed to further investigate the *in vivo* effects of glycation to confirm the mechanisms observed with *in vitro* glycation.

## 4. MATERIALS AND METHODS

### 4.1 Rat tail sample preparation.

Skeletally mature Brown Norway rats (20 weeks old, male) were euthanized by isoflurane inhalation for an unrelated study, according to state and federal regulations. Rat tails were removed and stored at -20°C until the day of the experiment, which has been shown not to affect tendon mechanics [50]. Individual rat tail tendon fascicles (RTTFs) were gently extracted from the middle region of the tail, subsequently cut into two equal parts and assigned either to the glycated group or to the non-glycated control for paired analysis. In specimens of the glycated group, AGEs were induced by incubation with 1 M D-ribose (Sigma-Aldrich, R7500) in Dulbecco's Modified Eagle's Medium (DMEM, Sigma-Aldrich, D6429) supplemented with 10% Fetal Bovine Serum (FBS, Gibco, 10270), 1% Penicillin Streptomycin (Sigma-Aldrich, P4333), 1% non-essential amino acids (Sigma-Aldrich, M7145) and 0.1%  $\beta$ -Mercaptoethanol (Sigma-Aldrich, M6250). RTTFs

of the non-glycated group were incubated in DMEM containing the same components as for the glycated group but without D-ribose. All samples were incubated under sterile conditions at 29°C for 12 days in a temperature-controlled incubator (5% CO<sub>2</sub>, 70% humidity).

#### **4.2 Human tendon sample preparation.**

All human tissue collection and experiments performed for this study were approved by the Ethical Review Board of the Canton of Zurich, and informed consent was given by all donors. Tendon tissue samples were obtained either from excess tendon graft material used in the reconstruction of the knee ligaments (semitendinosus, gracilis tendons) or from full tendons dissected from amputated extremities of diabetic patients. Tendons were stored at -20°C in PBS soaked gauze and used solely for the SAXS experiments. Samples were prepared immediately before the experiment by cutting a small piece of tissue (3 mm x 1 mm x 30 mm) using published methods [51, 52]. A few layers of paper were glued at the terminal ends (5 mm on both sides) to protect the tendon during clamping.

#### **4.3 AGEs quantification by collagen associated fluorescence.**

A fluorometric assay was carried out to assess the effects of the ribose treatment on the formation of AGEs in RTTFs and the different level of AGEs in tissues from human donors [36, 53]. Ribose treated, ribose control fascicles and samples from human donors were vacuum dried (RTTF: 16 h, human: 30h) to determine the dry weight and then digested (RTTF: 16 h, human: 72h) at 65°C with 0.2 mg/ml papain (Sigma-Aldrich, P4762) in PBE buffer (100 mM phosphate, 10 mM EDTA, pH 6.5) [53]. After centrifuging the samples at 8000 g for 1 h, triplicate aliquots of all supernatants were assayed for fluorescence using a microplate spectrofluorometer (SPECTRAMax GEMINI XS, Molecular Device, USA). Sample fluorescence was measured using 328 nm excitation (ex) and 378 nm emission (em), corresponding to the wavelengths used to detect and quantify pentosidine, the major crosslinking AGE resulting from ribose glycation [49]. The fluorescence readings were normalized to the dry weight of the samples.

#### **4.4 Photobleaching-coupled mechanical testing.**

We used photobleached lines made on the surface of collagen fascicles with confocal microscope in order to investigate single fiber stretching and sliding in stress relaxation tests, and in particular to assess the effect of AGEs on tissue micromechanics.

Following AGE induction, the extracellular matrix (ECM) of RTTFs (n = 8) was stained. Each fascicle was incubated for 20 min at room temperature in a 5-(4, 6-Dichlorotriazinyl) Aminofluorescein (5-DTAF, Life Technologies, D16) solution (100 µg/ml 5-DTAF and 0.1 M sodium bicarbonate buffer at pH 9.0). This ECM fluorescent dye binds to free amine groups of collagen and it has been used in previous publications to visualize collagen tissues [41, 42, 54].

The sample was then mounted on a custom-designed tensile stretching device consisting of two motorized linear stages (Zaber Technologies Inc., A-LSQ075A-E01) and a 20 N load cell (Transmetra GmbH, KD24S), placed on the stage of an iMic spinning disc confocal microscope (FEI/Till Photonics) equipped with a Hamamatsu Flash 4.0 sCMOS camera and a SOLE-6 Quad laser (Omicron) (Fig. 9A1). The RTTF was immersed in a PBS bath to maintain tissue hydration throughout the experiment. The cross-sectional area and the initial length  $L_0$  (from clamp-to-clamp) of the sample were measured at collagen fiber crimp (macroscopic fascicle waviness) disappearance. The tissue strain was defined as strain  $\epsilon_T = (L - L_0)/L_0$  in percentage, with L being the sample length. Before all mechanical tests, the RTTF was preconditioned ten times up to 1.0%  $L_0$ . Subsequently, at  $L_0$  two sets of five lines separated by 100 µm were photobleached onto the fascicle's surface in the central region of the sample with a 488 nm diode laser (Fig. 9A2). Such an approach has been used in previous studies to investigate local mechanics in collagen tissues [41-43]. At

this point, relaxation experiment was conducted, applying strains from 0 to 6%  $L_0$  to each sample at 0.6%  $L_0$  increments with a constant strain-rate of 0.5%  $L_0/s$  and a relaxation period of 200 s. The force readings were normalized to tissue stress by the cross-sectional area. At every strain increment image stacks (200 planes, 1  $\mu\text{m}$  distance between planes, 1024 x 2660 px) of the collagen matrix with photobleached lines (488 nm excitation, 516 nm emission) were taken after a relaxation period of 60s (majority of relaxation) using a 10X objective (Olympus, UPLSAPO, N.A. 0.4). Due to the curved surface of the fascicle, image stacks were necessary.

#### 4.5 Image Analysis.

After the image acquisition, Z-stacks were converted to single composite images using the standard deviation projection method in ImageJ (v1.49p). ECM deformation was assessed by image post-processing of the photobleached lines, based on Szczesny and Elliott [42]. Briefly, pixel intensities of the composite image were acquired with a custom Matlab algorithm (Fig. S4A). The location of the five photobleached lines (lowest intensity) was used to determine fiber strain and interfiber sliding (Fig. S4B). Fiber strain was calculated as the change in distance between two neighboring lines. Interfiber sliding was determined as the angle ( $\alpha$ ) between each photobleached line and the direction perpendicular to the fascicle axis (y-direction). The overall amount of interfiber sliding was calculated from the spread of the computed angle, i.e. the standard deviation was determined of the angle averaged across the five photobleached lines (Fig. S4C). The fiber strain and interfiber sliding averaged across the two sets of photobleached lines were used for statistical analysis.

#### 4.6 Mechanical testing coupled with small-angle X-ray scattering.

SAXS coupled with mechanical testing was used to investigate the effects of glycation at the fibril and molecular level during ramp-to-failure and relaxation experiments. Collagen fibril deformation during tendon tensile loading was measured at the coherent small-angle X-ray scattering beamline at the Swiss Light Source, Paul Scherrer Institute, Switzerland. Paired RTTFs ( $n=8$ ) were tested after incubation in control solution or in the presence of 1 M ribose for 12 days.

Following sample preparation, as described before, fascicle-clamp assemblies were mounted on a custom-built tensile testing apparatus (linear stepper motor: NA23C60, accuracy 40  $\mu\text{m}$ , Zaber Technologies Inc., Vancouver, Canada; load cell: KD24S, 20 N, accuracy: 0.1 %, Transmetra, Switzerland) with a custom-designed control software (LabVIEW, National Instruments). A precision X-Y table was used to adjust the axial sample alignment. The tensile tester was a modification of an available micro-compression device [55], which was designed to fit on the stage of the coherent small-angle X-ray scattering (cSAXS) beamline at Swiss Light Source (Paul Scherrer Institute, Switzerland). During all experiments two 4  $\mu\text{m}$  Ultralene films (X-ray semitransparent material) were placed on two sides of each tendon held together by a drop of PBS to maintain tissue hydration [56].

To measure collagen fibril deformation during tendon loading we used SAXS with a X-ray wavelength of 0.1 nm obtained from a double-crystal Si (111) monochromator and a beam cross-section at the sample 340  $\mu\text{m}$  width and 300  $\mu\text{m}$  height obtained by slight focusing using bendable monochromator crystal and high-order rejection mirror. The specimens were placed  $\sim 12$  mm upstream the entrance window of an evacuated 2.1 m flight tube. 2D diffraction patterns were recorded with an in-house developed PILATUS 2M detector (array size: 1475 x 1679 pixels; pixel size: 172 x 172  $\mu\text{m}^2$ ; active area: 254x289  $\text{mm}^2$ ) [57]. The total sample to detector distance (2.178 m) and the center of the direct beam on the detector were calibrated using silver behenate. During ramp-to-failure tests, the SAXS frames were collected with an acquisition time of 200 ms concurrently during mechanical testing with the Pilatus detector being triggered

by the testing apparatus software via TTL pulses. Conversely, during stress relaxation experiments the frames were acquired at exponentially increasing time intervals subsequent tissue strain increments of  $De_T = 0.6 \% L_0$  (up to  $3\% L_0$ ) This exponential curve matched previous published collagen fibril relaxation by Gupta [56] and allowed a most optimal acquisition of data where collagen deformation occurred. A shutter closing between frames reduced the X-ray dose at the sample.

The collected 2D SAXS patterns showed the 2<sup>nd</sup> to 36<sup>th</sup> order equatorial collagen reflections due to the D-banding and the meridional reflection due to molecular spacing (Fig. 9B1). Azimuthal integration was carried out over angular sectors of  $22.5^\circ$  width centered at the calibrated location of the direct beam on the detector. From the resulting 1D intensity profiles [averaged photons per pixel] versus  $q$  [ $\text{nm}^{-1}$ ] a two term exponential background was subtracted (empirically determined best fit). The equatorial peak position, height and width (FWHM) were estimated by fitting a series of Gaussian curves to the first 8 order collagen reflections using non-linear least squares (OriginPro 8.6; Matlab R2013a) (Fig. 9B2,4). The collagen fibril D-spacing was calculated as  $D = 2\pi/\Delta q$ , where  $\Delta q$  is the average spacing between the peak positions. Either absolute or normalized change of D-spacing served as averaged measures of collagen fibril elongation: collagen fibril deformation ( $\Delta D = D - D_0$ ) and collagen fibril strain ( $e_F = D / D_0 - 1$  [%]) with  $D_0$  as D-period length at pre-stress/start of experiment. For each relaxation step, collagen fibril relaxation was measured as the relative shortening of the D-period length normalized to the D-period length ( $D_{0,s}$ ) at start of the relaxation step:  $De_F = D / D_{0,s} - 1$  [%]. The meridional peak position, height and width (FWHM) was estimated by fitting a single Gaussian curve and the molecular distance calculated as  $d = 2\pi/q$  (Fig. 9B3).

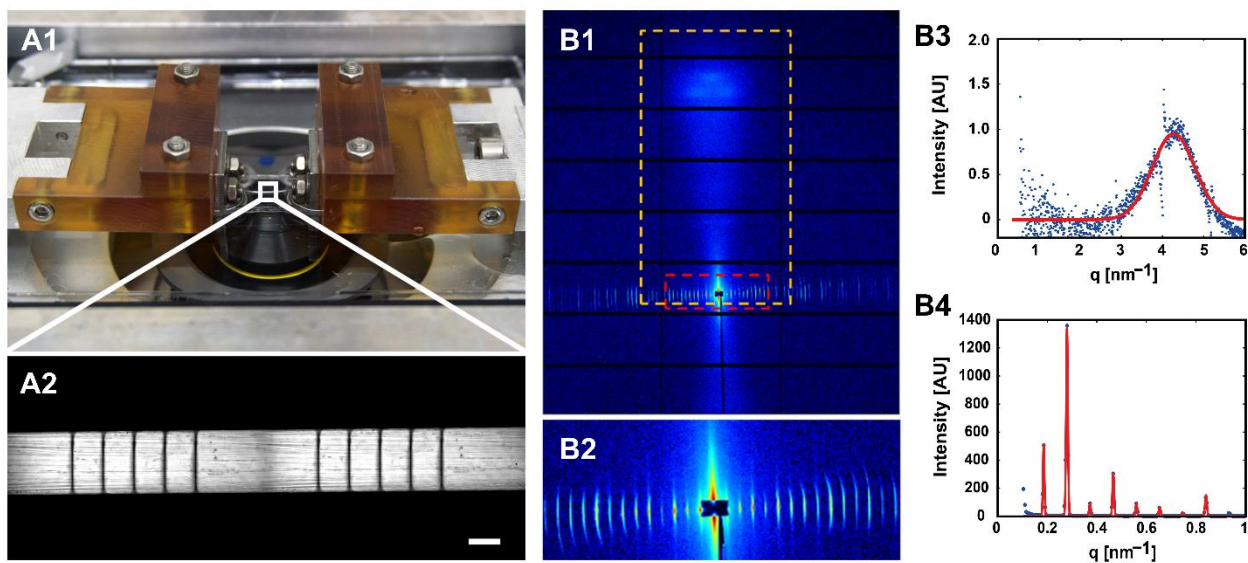


**Figure 9. Advanced multiscale imaging techniques.** (A) Experimental setup for matrix level mechanical tests: RTTFs were clamped in a custom stretching device mounted on the stage of a confocal microscope (A1). Representative monochrome image showing the two sets of five photobleached lines to track collagen fiber sliding and stretch (A2). Scale bar represents  $100 \mu\text{m}$ . (B) SAXS experiments: the 2D SAXS diffraction pattern (B1) recorded from tendons are dominated by the strong meridional reflection of a spacing about  $\approx 1.4 \text{ nm}$  and by the equatorial meridional Bragg reflections corresponding to  $\approx 67.5 \text{ nm}$  and harmonic frequencies of this spacing (B2). The meridional reflections (yellow square) are used to determine the molecular spacing (B3), while the equatorial intensities (red square) are integrated azimuthally, which resulted in 1-D intensity profiles ( $q$  [ $\text{nm}^{-1}$ ] vs.  $I$  [average photons per pixel]). The equatorial peak positions (red square) are used to calculate the length of the D-period (B4). Changes of the peak spacing served then as averaged measure for collagen fibril elongation or changes in molecular spacing.

#### **4.7 Statistical Analysis.**

Parameters derived from the experiments on RTT fascicles were analyzed using two tailed unpaired student T-tests, one-way ANOVAs and two-way ANOVAs. Correlation between age and human tissue parameters were assessed through Pearson's coefficient. Statistically significant differences were defined as  $p < 0.05$  (indicated with an asterisk in the figures). Results were reported as means  $\pm$  standard deviations. All statistical analyses were performed with GraphPad Prism 6.

### **5. ACKNOWLEDGMENTS**

The authors gratefully acknowledge the excellent work of Marco Hitz from the Institute for Biomechanics of ETH Zurich in adapting the tensile testing device to suit the SAXS experiments. We also thank Remo Bernet for his expertise and contribution to the image analysis and Dr. Philipp Kron for providing the rat tails used for our experiments. Further, we gratefully acknowledge Stefania Wunderli, Aron Horvath, Claude Holenstein, Tojo Razafiarison, Elias Bachman, Amro Hussien and Massimo Bagnani for performing parts of the mechanical testing. This work has been partially supported by Fondazione Cariplo, grant n° 2013-0766 and Swiss National Science Foundation grant number IZK0Z3\_154235.

## 6. REFERENCES

- [1] A.J. Bailey, Molecular mechanisms of ageing in connective tissues, *Mechanisms Of Ageing And Development* 122(7) (2001) 735-755.
- [2] J.G. Snedeker, A. Gautieri, The role of collagen crosslinks in ageing and diabetes - the good, the bad, and the ugly, *Muscles, ligaments and tendons journal* 4(3) (2014) 303-8.
- [3] N.A. Ansari, D. Dash, Amadori glycated proteins: role in production of autoantibodies in diabetes mellitus and effect of inhibitors on non-enzymatic glycation, *Aging Dis* 4(1) (2013) 50-6.
- [4] D.G. Dyer, J.A. Dunn, S.R. Thorpe, K.E. Bailie, T.J. Lyons, D.R. McCance, J.W. Baynes, Accumulation of Maillard reaction products in skin collagen in diabetes and aging, *J Clin Invest* 91(6) (1993) 2463-9.
- [5] M. Sensi, F. Pricci, G. Pugliese, M.G. De Rossi, A.F. Petrucci, A. Cristina, S. Morano, G. Pozzessere, E. Valle, D. Andreani, et al., Role of advanced glycation end-products (AGE) in late diabetic complications, *Diabetes Res Clin Pract* 28(1) (1995) 9-17.
- [6] S. Yamagishi, Role of advanced glycation end products (AGEs) and receptor for AGEs (RAGE) in vascular damage in diabetes, *Exp Gerontol* 46(4) (2011) 217-24.
- [7] N.C. Avery, A.J. Bailey, The effects of the Maillard reaction on the physical properties and cell interactions of collagen, *Pathol Biol* 54(7) (2006) 387-95.
- [8] N. Verzijl, J. DeGroot, S.R. Thorpe, R.A. Bank, J.N. Shaw, T.J. Lyons, J.W.J. Bijlsma, F.P.J.G. Lafeber, J.W. Baynes, J.M. TeKoppele, Effect of collagen turnover on the accumulation of advanced glycation end products, *Journal of Biological Chemistry* 275(50) (2000) 39027-39031.
- [9] B.H. Toyama, M.W. Hetzer, OPINION Protein homeostasis: live long, won't prosper, *Nat Rev Mol Cell Bio* 14(1) (2013) 55-61.
- [10] T.T. Andreassen, K. Seyerhansen, A.J. Bailey, Thermal-Stability, Mechanical-Properties and Reducible Cross-Links of Rat Tail Tendon in Experimental Diabetes, *Biochimica Et Biophysica Acta* 677(2) (1981) 313-317.
- [11] S.L. Schnider, R.R. Kohn, Effects of Age and Diabetes-Mellitus on the Solubility of Collagen from Human-Skin, Tracheal Cartilage and Dura Mater, *Exp Gerontol* 17(3) (1982) 185-194.
- [12] T. Su, L. Xin, Y.G. He, Y. Wei, Y.X. Song, W.W. Li, X.M. Wang, R.Q. He, The Abnormally High Level of Uric D-Ribose for Type-2 Diabetics, *Prog Biochem Biophys* 40(9) (2013) 816-825.
- [13] S.K. Grandhee, V.M. Monnier, Mechanism of Formation of the Maillard Protein Cross-Link Pentosidine - Glucose, Fructose, and Ascorbate as Pentosidine Precursors, *Journal of Biological Chemistry* 266(18) (1991) 11649-11653.
- [14] D.R. Sell, K.M. Biemel, O. Reihl, M.O. Lederer, C.M. Strauch, V.M. Monnier, Glucosepane is a major protein cross-link of the senescent human extracellular matrix. Relationship with diabetes, *J Biol Chem* 280(13) (2005) 12310-5.
- [15] V.M. Monnier, G.T. Mustata, K.L. Biemel, O. Reihl, M.O. Lederer, Z.Y. Dai, D.R. Sell, Cross-linking of the extracellular matrix by the Maillard reaction in aging and diabetes - An update on "a puzzle nearing resolution", *Ann Ny Acad Sci* 1043 (2005) 533-544.

- [16] K.L. Reigle, G. Di Lullo, K.R. Turner, J.A. Last, I. Chervoneva, D.E. Birk, J.L. Funderburgh, E. Elrod, M.W. Germann, C. Surber, R.D. Sanderson, J.D.S. Antonio, Non-enzymatic glycation of type I collagen diminishes collagen-proteoglycan binding and weakens cell adhesion, *J Cell Biochem* 104(5) (2008) 1684-1698.
- [17] A. Gautieri, A. Redaelli, M.J. Buehler, S. Vesentini, Age- and diabetes-related nonenzymatic crosslinks in collagen fibrils: Candidate amino acids involved in Advanced Glycation End-products, *Matrix Biol* (2013).
- [18] A. Gautieri, S. Vesentini, A. Redaelli, R. Ballarini, Modeling and measuring visco-elastic properties: From collagen molecules to collagen fibrils, *Int J Nonlin Mech* 56 (2013) 25-33.
- [19] S. Vesentini, A. Redaelli, A. Gautieri, Nanomechanics of collagen microfibrils, *Muscles Ligaments Tendons J* 3(1) (2013) 23-34.
- [20] N. Verzijl, J. DeGroot, C. Ben Zaken, O. Braun-Benjamin, A. Maroudas, R.A. Bank, J. Mizrahi, C.G. Schalkwijk, S.R. Thorpe, J.W. Baynes, J.W.J. Bijlsma, F.P.J.G. Lafeber, J.M. TeKoppele, Crosslinking by advanced glycation end products increases the stiffness of the collagen network in human articular cartilage - A possible mechanism through which age is a risk factor for osteoarthritis, *Arthritis and Rheumatism* 46(1) (2002) 114-123.
- [21] R.B. Svensson, H. Mulder, V. Kovanen, S.P. Magnusson, Fracture Mechanics of Collagen Fibrils: Influence of Natural Cross-Links, *Biophysical Journal* 104(11) (2013) 2476-2484.
- [22] S.Y. Tang, D. Vashishth, The relative contributions of non-enzymatic glycation and cortical porosity on the fracture toughness of aging bone, *Journal of Biomechanics* 44(2) (2011) 330-336.
- [23] D.R. Sell, V.M. Monnier, Molecular Basis of Arterial Stiffening: Role of Glycation - A Mini-Review, *Gerontology* 58(3) (2012) 227-237.
- [24] S. Del Turco, G. Basta, An update on advanced glycation endproducts and atherosclerosis, *Biofactors* 38(4) (2012) 266-274.
- [25] S.Y. Goh, M.E. Cooper, The role of advanced glycation end products in progression and complications of diabetes, *J Clin Endocr Metab* 93(4) (2008) 1143-1152.
- [26] R.H. Nagaraj, M. Linetsky, A.W. Stitt, The pathogenic role of Maillard reaction in the aging eye, *Amino Acids* 42(4) (2012) 1205-1220.
- [27] A.M. Vincent, J.W. Russell, P. Low, E.L. Feldman, Oxidative stress in the pathogenesis of diabetic neuropathy, *Endocr Rev* 25(4) (2004) 612-628.
- [28] M.R. Dressler, D.L. Butler, R. Wenstrup, H.A. Awad, F. Smith, G.P. Boivin, A potential mechanism for age-related declines in patellar tendon biomechanics, *J Orthopaed Res* 20(6) (2002) 1315-1322.
- [29] A. Bedi, A.J.S. Fox, P.E. Harris, X.H. Deng, L.A. Ying, R.F. Warren, S.A. Rodeo, Diabetes mellitus impairs tendon-bone healing after rotator cuff repair, *J Shoulder Elb Surg* 19(7) (2010) 978-988.
- [30] P. Hansen, B.T. Haraldsson, P. Aagaard, V. Kovanen, N.C. Avery, K. Qvortrup, J.O. Larsen, M. Krogsgaard, M. Kjaer, S.P. Magnusson, Lower strength of the human posterior patellar tendon seems unrelated to mature collagen cross-linking and fibril morphology, *J Appl Physiol* 108(1) (2010) 47-52.
- [31] R.B. Svensson, P. Hansen, T. Hassenkam, B.T. Haraldsson, P. Aagaard, V. Kovanen, M. Krogsgaard, M. Kjaer, S.P. Magnusson, Mechanical properties of human patellar tendon at the hierarchical levels of tendon and fibril, *J Appl Physiol* 112(3) (2012) 419-426.

- [32] D.A. Slatter, N.C. Avery, A.J. Bailey, Collagen in its fibrillar state is protected from glycation, *Int J Biochem Cell Biol* 40(10) (2008) 2253-63.
- [33] Y. Li, G. Fessel, M. Georgiadis, J.G. Snedeker, Advanced glycation end-products diminish tendon collagen fiber sliding, *Matrix Biol* (2013).
- [34] E.A. Zimmermann, E. Schaible, H. Bale, H.D. Barth, S.Y. Tang, P. Reichert, B. Busse, T. Alliston, J.W. Ager, R.O. Ritchie, Age-related changes in the plasticity and toughness of human cortical bone at multiple length scales, *Proceedings of the National Academy of Sciences of the United States of America* 108(35) (2011) 14416-14421.
- [35] D. Vashishth, G.J. Gibson, J.I. Khoury, M.B. Schaffler, J. Kimura, D.P. Fyhrie, Influence of nonenzymatic glycation on biomechanical properties of cortical bone, *Bone* 28(2) (2001) 195-201.
- [36] G. Fessel, Y.F. Li, V. Diederich, M. Guizar-Sicairos, P. Schneider, D.R. Sell, V.M. Monnier, J.G. Snedeker, Advanced Glycation End-Products Reduce Collagen Molecular Sliding to Affect Collagen Fibril Damage Mechanisms but Not Stiffness, *Plos One* 9(11) (2014).
- [37] A. Gautieri, S. Vesentini, A. Redaelli, M.J. Buehler, Hierarchical Structure and Nanomechanics of Collagen Microfibrils from the Atomistic Scale Up, *Nano Letters* 11(2) (2011) 757-766.
- [38] P. Fratzl, *Collagen: Structure and Mechanics*, Springer, New York, 2008.
- [39] N. Sasaki, S. Odajima, Elongation mechanism of collagen fibrils and force-strain relations of tendon at each level of structural hierarchy, *Journal Of Biomechanics* 29(9) (1996) 1131-1136.
- [40] Y.F. Li, G. Fessel, M. Georgiadis, J.G. Snedeker, Advanced glycation end-products diminish tendon collagen fiber sliding, *Matrix Biol* 32(3-4) (2013) 169-177.
- [41] V.W.T. Cheng, H.R.C. Screen, The micro-structural strain response of tendon, *J Mater Sci* 42(21) (2007) 8957-8965.
- [42] S.E. Szczesny, D.M. Elliott, Interfibrillar shear stress is the loading mechanism of collagen fibrils in tendon, *Acta Biomaterialia* 10(6) (2014) 2582-2590.
- [43] C.T. Thorpe, C. Klemm, G.P. Riley, H.L. Birch, P.D. Clegg, H.R. Screen, Helical sub-structures in energy-storing tendons provide a possible mechanism for efficient energy storage and return, *Acta Biomater* 9(8) (2013) 7948-56.
- [44] M. Lavagnino, M.E. Wall, D. Little, A.J. Banes, F. Guilak, S.P. Arnoczky, Tendon mechanobiology: Current knowledge and future research opportunities, *Journal of orthopaedic research : official publication of the Orthopaedic Research Society* 33(6) (2015) 813-22.
- [45] X. Wu, V.M. Monnier, Enzymatic deglycation of proteins, *Arch Biochem Biophys* 419(1) (2003) 16-24.
- [46] F. Rigoldi, A. Gautieri, A. Dalle Vedove, A.P. Lucarelli, S. Vesentini, E. Parisini, Crystal structure of the deglycating enzyme amadoriase i in its free form and substrate-bound complex, *Proteins* (2016).
- [47] G.E. Sroga, A. Siddula, D. Vashishth, Glycation of human cortical and cancellous bone captures differences in the formation of Maillard reaction products between glucose and ribose, *Plos One* 10(2) (2015) e0117240.
- [48] G.K. Reddy, Cross-linking in collagen by nonenzymatic glycation increases the matrix stiffness in rabbit achilles tendon, *Experimental diabetes research* 5(2) (2004) 143-53.

- [49] T.L. Willett, S. Suttly, A. Gaspar, N. Avery, M. Grynypas, In vitro non-enzymatic ribation reduces post-yield strain accommodation in cortical bone, *Bone* 52(2) (2013) 611-622.
- [50] K.L. Goh, Y. Chen, S.M. Chou, A. Listrat, D. Bechet, T.J. Wess, Effects of frozen storage temperature on the elasticity of tendons from a small murine model, *Animal : an international journal of animal bioscience* 4(9) (2010) 1613-7.
- [51] G. Fessel, J. Wernli, Y.F. Li, C. Gerber, J.G. Snedeker, Exogenous collagen cross-linking recovers tendon functional integrity in an experimental model of partial tear, *J Orthopaed Res* 30(6) (2012) 973-981.
- [52] G. Fessel, J. Wernli, Y. Li, C. Gerber, J.G. Snedeker, Exogenous collagen cross-linking recovers tendon functional integrity in an experimental model of partial tear, *Journal of orthopaedic research : official publication of the Orthopaedic Research Society* 30(6) (2012) 973-81.
- [53] S.Y. Tang, U. Zeenath, D. Vashishth, Effects of non-enzymatic glycation on cancellous bone fragility, *Bone* 40(4) (2007) 1144-51.
- [54] S.E. Szczesny, R.S. Edelstein, D.M. Elliott, DTAF Dye Concentrations Commonly Used to Measure Microscale Deformations in Biological Tissues Alter Tissue Mechanics, *Plos One* 9(6) (2014).
- [55] M. Meier, P. Vogel, R. Voide, P. Schneider, R. Muller, Investigation of microdamage in murine bone under dynamic load, *J Biomech* 41 (2008).
- [56] H.S. Gupta, J. Seto, S. Krauss, P. Boesecke, H.R. Screen, In situ multi-level analysis of viscoelastic deformation mechanisms in tendon collagen, *Journal of structural biology* 169(2) (2010) 183-91.
- [57] P. Kraft, A. Bergamaschi, C. Bronnimann, R. Dinapoli, E.F. Eikenberry, H. Graafsma, B. Henrich, I. Johnson, M. Kobas, A. Mozzanica, C.A. Schleputz, B. Schmitt, Characterization and Calibration of PILATUS Detectors, *IEEE T Nucl Sci* 56(3) (2009) 758-764.